Large superconducting spin valve effect and ultra-small exchange-splitting in epitaxial rare-earth-niobium trilayers

Yuanzhou Gu,[1,*] Gábor B. Halász,[2] J. W. A. Robinson,[1] and M. G. Blamire[1]

[1]Department of Materials Science and Metallurgy, University of Cambridge,
27 Charles Babbage Road, Cambridge, CB3 0FS, United Kingdom
[2]Theoretical Physics, Oxford University, 1 Keble Road, Oxford OX1 3NP, United Kingdom

Epitaxial Ho/Nb/Ho and Dy/Nb/Dy superconducting spin valves (SSVs) show a reversible change in the zero-field critical temperature (ΔT_{c0}) of ~400 mK and an infinite magnetoresistance on changing the relative magnetization of the Ho or Dy layers. Unlike transition metal SSVs which show much smaller ΔT_{c0} values, our results can be quantitatively modeled. However, the fits require an extraordinarily low induced exchange splitting which is dramatically lower than known values for rare-earth Fermi-level electrons implying that new models for the magnetic proximity effect may be required.

Superconducting spintronics has become an emerging field that holds great potential for high speed information processing with low energy consumption [1]. The superconducting spin valve (SSV) exploits proximity-coupling between a superconductor and two ferromagnet (F) layers such that the exchange-induced suppression of the critical temperature (T_c) is controlled by the relative magnetization orientation of the F layers [2–5]. To date, experimental realization of this effect [6–22] has been limited to transition metal (TM) F layers and the maximum ΔT_c between parallel (P) and antiparallel (AP) orientation is about 40 mK, with a T_c below 0.4 K [9]. Although ΔT_c was improved to 200 mK with a T_c around 2.8 K, this was obtained in a large (kOe) field [10]. In all cases ΔT_c is much smaller than theoretically predicted.

Previously, we studied the proximity effect by using an epitaxial Ho film and observed a zero-field ΔT_c (ΔT_{c0}) of Nb ~ 120 mK with a T_c in the range of 6~7 K [23], but this was based on the irreversible metamagnetic phase transformation of the Ho between spin-spiral (S) and F states. In this Letter we report results from SSVs comprising two epitaxial rare earth (RE) films sandwiching epitaxial Nb which showed a large $\Delta T_{c0} \approx 700$ mK between S and P states and a reversible $\Delta T_{c0} \approx 400$ mK between P and AP states. To eliminate any possible effect of stray fields, we also studied Dy/Nb/Dy SSVs since Dy does not show any magnetic out-of-plane component in bulk.

All films were grown by DC magnetron sputtering on a-plane (110) sapphire substrates as described previously [23]. The inset in Fig. 1 shows the layer structure in which the top Ho layer thickness d = 10, 40, and 70 nm. The bottom and top Nb layers are respectively a seed layer and capping layer; both are non-superconducting. Magnetic measurements were performed at 10 K using a vibrating sample magnetometer (VSM), and transport measurements were carried out in a liquid helium cryostat (down to 1.5 K) with the standard four-point geometry. A typical in-plane (IP) magnetic moment vs. magnetic field ($M(H)$) loop of a SSV (d = 40 nm) at 10 K is shown in Fig. 1. The magnetic moment at 0.6 T is ~ 2500 emu cm^{-3}, which is close to that previously reported for epitaxial Ho [23]. This confirms that both top and bottom Ho films are epitaxial because the moment of non-epitaxial Ho films is one order of magnitude smaller. Importantly, because the coercivities of Ho films vary with thickness, the magnetization directions of two Ho films can be aligned either P or approximately AP as indicated by the arrows in Fig. 1.

To investigate the SSV effect, we measured the zero-field resistance vs. temperature *($R_0(T)$)* curves with different field histories. In each case we define the set field ($\mu_o H_{set}$) as the field applied and then removed before each sequential $R_0(T)$ measurement is taken. Figure 2 (a) shows T_{c0} (H_{set}) - T_{c0} (S) vs $\mu_o H_{set}$ for a typical SSV. We define T_{c0} as the zero-field temperature where the resistance drops to 50% of the residual resistance. Previously we showed a continuous field-driven phase transformation from the S to F state for epitaxial Ho films through which the T_{c0} of a Nb/Ho bilayer could be gradually suppressed [23]. This can be seen in the initial response in Fig. 2(a) in which T_{c0} (H_{set}) - T_{c0} (S) increases with successive $\mu_o H_{set}$ until the phase transformation is complete at $\mu_o H_{set} \sim 1$ T. At this point the Ho films are F and P, and $\Delta T_{c0} \approx 700$ mK relative to the S state. Subsequently, ΔT_{c0} varies reversibly by 400 mK between P and AP states as $\mu_o H_{set}$ is cycled between ± 1 T. The peaks at ± 0.1 T correspond to an AP alignment, in good agreement with the magnetic measurement shown in Fig. 1. Figure 2(b) shows representative $R_0(T)$ curves measured at three specific states: S, P, and AP.

As ΔT_{c0} is very large, we can choose a temperature at which the device can be switched between the AP superconducting and P non-superconducting state. Figure 2(c) shows *R(H)*: at 3 K the SSV is in the normal state when the field is at ± 1 T but at ± 0.1 T the SSV reaches a fully superconducting state and, therefore, an infinite magnetoresistance (MR = $\Delta R/R_{min}$) is achieved. This figure also shows that MR progressively reduces with increasing temperature.

We summarize T_{c0} of various SSVs in Fig. 3(a). Since it is easier to keep the entire SSV structure epitaxial when the base Ho is thin, we changed only the thickness of the top Ho layer. It is clear that T_{c0} of SSVs decreases continuously as the thickness of the top Ho layer is increased from 10 to 70 nm. To eliminate any possible contribution of stray flux-induced T_c suppression arising from an out-of-(basal) plane (OOP) magnetisation which may be enhanced in thick Ho films [24], OOP magnetic measurements were performed: data for a d = 70 nm SSV shown in inset (a) gives no evidence for a zero-field magnetization. We also replaced Ho with Dy which has no OOP component in bulk and observed similar behavior with a gradual decay of T_{c0} and increase in ΔT_{c0} as the Dy thickness is increased (Fig. 3(b)).

We should point out that there is no well-defined AP state for SSVs when two Ho (or Dy) layers have the same thickness since this does not give rise to a difference in coercivity. The small T_{c0} shift of 'AP' relative to P in d = 10 nm SSVs may come from the generation of domains at the coercive field, but this effect is small compared with the SSV effect. We also made Ho (10 nm)/Nb/Dy (10 nm) SSV because Ho and Dy have different coercivities. However, the SSV effect is also ~ 110 mK. This proves that the SSV effect is related to the thickness of RE.

So far, we have demonstrated a much larger ΔT_{c0} in comparison with TM SSVs together with an infinite MR. We now discuss the origins of these remarkable features. First we focus on ΔT_{c0}; theoretical predictions [3,4] for TM SSVs ΔT_{c0} in the dirty limit can be two orders of magnitude higher than the corresponding experimental results [10,19]. To compare our results with theory, we used the Usadel equation to model our results in the dirty limit because the mean free paths of both epitaxial Nb and Ho (l_{Nb}, l_{Ho}) were smaller than their respective coherence lengths (ξ_{Nb}, ξ_{Ho}) [23]. In this model, the T_{c0} of the three states (S, P, AP) were found by solving the linearized Usadel equation via a self-consistent numerical procedure [44]. We modeled Ho as a non-magnetic metal in the S state (assuming that its exchange field averages to zero within ξ_{Ho}) and as a homogeneous F metal in the P and AP states. To obtain the theoretical fits shown in Fig. 3(c), we used the experimental values of d_{Nb} and d_{Ho}, as well as the bulk Nb T_c = 9.2 K. The following parameters were then adjusted to optimize

the fit: the Fermi velocities $v_{Nb} = 0.6 \times 10^6$ m/s and $v_{Ho} = 2.0 \times 10^6$ m/s, the electron mean free paths l_{Nb} = 10 nm and l_{Ho} = 5 nm, the dimensionless Nb/Ho interfacial resistance $\gamma_b = R_{Nb/Ho}\, \sigma_{Ho} / \xi_{Ho} \sim 0.3$ (where $R_{Nb,Ho}$ is the interfacial resistance, σ_{Ho} is the normal-state Ho conductivity, and $\xi_{Ho} \sim 30$ nm is the Ho coherence length), and the Ho exchange energy E_{ex} = 1 meV in the P and AP states. Dy has no spiral phase, but we assume that the as-cooled virgin state has a domain size smaller than ξ_{Nb} [25] and the net exchange interaction will also average to zero. Thus we modeled the Dy/Nb/Dy SSVs with the same method for which the extracted parameters for Dy and the interface are in the same range.

Figure 3(c,d) and the insets show that the model can quantitatively describe the experimental results, ΔT_{c0} being especially well reproduced. The inset to Fig. 2(b) highlights the fact that the resistive transitions are significantly broadened; this can be accounted for in our model if we assume that this originates from magnetic inhomogeneity within and between the Ho layers. For example, local regions in which the Ho layers are not collinear or that retain the antiferromagnetic S state would have a higher local T_c than regions which are perfectly aligned. In fact the onset of the resistive transition occurs at approximately the same temperature for all samples implying that there are regions which do not transform into the F state.

The inset to Fig. 3(b) shows the sample to sample variation with a particular d_{Dy}, with different d_{Dy} samples being deposited in different runs. However, while most of the fitting parameters are within reasonable ranges [23], the exchange energy E_{ex} for both Ho and Dy is extraordinarily small (~ 1 meV). From the point of view of the modeling, it is clear that we require such a small E_{ex}. All curves in Fig. 3 have an exceptionally long decay length for a ferromagnetic system that translates into an extremely small exchange energy [26].

The REs have a complex magnetic structure with the 5*d*/6*s* bands exchange-split by the 4*f* electrons [27]. The polarization of 5*d* electrons contributes to RKKY coupling and leads to an additional magnetic moment [27–29]. Strikingly, E_{ex} extracted from the fit is several orders of magnitude smaller than the calculated and inferred 5*d*/6*s* and 4*f* exchange splitting for REs ~ 1 eV [30–32] and 10 eV [27,28,33], respectively. Because of the largely localized nature of the 4*f* electrons it is unsurprising that the E_{ex} required for fitting our data is much less than 10 eV, but this value is also much lower than that of the itinerant 5*d*/6*s* electrons. This is completely different from the situation of TM Fs for which there is good agreement between the exchange splitting of ferromagnetic band structures and extracted E_{ex}, both from SSVs [34] and SFS Josephson junctions [26]. We notice that the proximity of a F layer with a normal metal (N) layer may result in a reduction of the effective E_{ex} [35–37], so we also modeled a N/F/S/F/N structure [44] to study the effect of the seed and capping Nb layers. As a result, the values of T_c are slightly shifted but the overall conclusion remains the same with $E_{ex} \sim 1$ meV. Therefore, the issue of how to define the effective E_{ex} *as seen by the Cooper pairs* is a question which needs detailed consideration. While this paper cannot offer a definitive explanation, there appears to be two possible underlying reasons. The first is that although the *s* and *d* bands participate in the indirect coupling of the *f* electron moments, the exchange energy experienced by the conduction electrons themselves may be significantly less than the apparent band exchange splitting: for example interband mixing can explain the apparent negative exchange coupling seen in certain transport experiments [38].

Alternatively, there is the possibility of other pairing symmetries being involved in the superconducting coupling. Polycrystalline Ho has been shown to act as an effective spin mixer for the generation of odd-frequency triplet pairs [39] and an inverse spin valve effect, opposite in sign from

the conventional behavior [5–10] and seen in this study, has been reported as evidence for spin-aligned triplet pairing [40]. Of more direct relevance to this study, Point-contact Andreev reflection (PCAR) spectroscopy between a Nb tip and single crystal or epitaxial film samples of Ho shows an effective spin polarization arising from the Ho which decreases rapidly as the interface resistance decreases which may reflect an emergent triplet state [41].

Despite the ultra-small E_{ex} in comparison even with weak TM ferromagnets, we see a very large reversible $\Delta T_{c0} \approx 400$ mK which is in quantitative agreement with the theoretical model. Previous theories suggested that to get a sizable ΔT_{c0} it is crucial to have a high interface transparency, a small pair-breaking scattering, and a large superconducting coherence length because Cooper pairs have to sense the exchange field from both F layers [8,10,19]. The fully epitaxial nature of our SSVs should improve interface quality and hence provide a reasonably high interface transparency and a small interface scattering as evidenced by the small dimensionless interfacial resistance $\gamma_b \sim 0.3$. The results also imply very good band matching at the interface. Secondly, the large $\xi_{Ho} \sim 30$ nm gives rise to a small pair-breaking effect. Thirdly, we confirmed the Nb coherence length $\xi_{Nb} = 32$ nm [23], which is larger than $d_{Nb} = 20$ nm.

In fact, the behavior seen in our metallic SSVs is strikingly similar to that seen in ferromagnetic insulator/superconductor trilayer devices in terms of the magnitude of ΔT_c and the infinite MR [42]. However, the results for that system are explained in terms of the *large* exchange field induced in the superconductor and obviously no S/F transmission – i.e. apparently the opposite scenario to our results.

In conclusion, we constructed SSVs by using two epitaxial RE films with one epitaxial S film sandwiched in between. Ho/Nb/Ho SSVs showed a large $\Delta T_{c0} \approx 700$ mK between S and P states and a reversible $\Delta T_{c0} \approx 400$ mK between P and AP states. Apart from the SSV effect, we also observed infinite MR and a long-ranged superconducting behaviour. Dy/Nb/Dy SSVs showed similar behaviours. Although the theoretical model applied agrees well with the experimental results, the ultra-small extracted E_{ex} suggests that some degree of new physics is involved and a more advanced theory is thus required. Nevertheless, we have demonstrated a new type of SSV based on epitaxial REs and the remarkable features observed make them very promising for practical applications such as superconducting memory.

This work is partially supported by ERC AiG "Superspin". Yuanzhou Gu acknowledges financial support from King's College, Cambridge. We thank J. T. Chalker for helpful discussions.

*yg286@cam.ac.uk

[1] M. Eschrig, Phys. Today **64**, 43 (2011).

[2] S. Oh, D. Youm, and M. R. Beasley, Appl. Phys. Lett. **71**, 2376 (1997).

[3] L. R. Tagirov, Phys. Rev. Lett. **83**, 2058 (1999).

[4] A. I. Buzdin, A. V Vedyayev, and N. V Ryzhanova, Europhys. Lett. **48**, 686 (1999).

[5] C.-Y. You, Y. B. Bazaliy, J. Y. Gu, S.-J. Oh, L. M. Litvak, and S. D. Bader, Phys. Rev. B **70**, 014505 (2004).

[6] J. Y. Gu, C.-Y. You, J. S. Jiang, J. Pearson, Y. B. Bazaliy, and S. D. Bader, Phys. Rev. Lett. **89**, 267001 (2002).

[7] A. Potenza and C. H. Marrows, Phys. Rev. B **71**, 180503 (2005).

[8] K. Westerholt, D. Sprungmann, H. Zabel, R. Brucas, B. Hjörvarsson, D. A. Tikhonov, and I. A. Garifullin, Phys. Rev. Lett. **95**, 097003 (2005).

[9] I. C. Moraru, W. P. Pratt Jr, and N. O. Birge, Phys. Rev. Lett. **96**, 037004 (2006).

[10] G. Nowak, H. Zabel, K. Westerholt, I. Garifullin, M. Marcellini, A. Liebig, and B. Hjörvarsson, Phys. Rev. B **78**, 134520 (2008).

[11] G.-X. Miao, A. V. Ramos, and J. S. Moodera, Phys. Rev. Lett. **101**, 137001 (2008).

[12] P. Cadden-Zimansky, Y. B. Bazaliy, L. M. Litvak, J. S. Jiang, J. Pearson, J. Y. Gu, C.-Y. You, M. R. Beasley, and S. D. Bader, Phys. Rev. B **77**, 184501 (2008).

[13] P. V. Leksin, N. N. Garif'yanov, I. A. Garifullin, J. Schumann, H. Vinzelberg, V. Kataev, R. Klingeler, O. G. Schmidt, and B. Büchner, Appl. Phys. Lett. **97**, 102505 (2010).

[14] J. Zhu, I. N. Krivorotov, K. Halterman, and O. T. Valls, Phys. Rev. Lett. **105**, 207002 (2010).

[15] P. V. Leksin, N. N. Garif'yanov, I. A. Garifullin, J. Schumann, V. Kataev, O. G. Schmidt, and B. Büchner, Phys. Rev. Lett. **106**, 067005 (2011).

[16] P. V. Leksin, N. N. Garif'yanov, I. A. Garifullin, J. Schumann, V. Kataev, O. G. Schmidt, and B. Büchner, Phys. Rev. B **85**, 024502 (2012).

[17] P. V. Leksin, A. A. Kamashev, N. N. Garif'yanov, I. A. Garifullin, Y. V. Fominov, J. Schumann, C. Hess, V. Kataev, and B. Büchner, JETP Lett. **97**, 478 (2013).

[18] V. I. Zdravkov, J. Kehrle, G. Obermeier, D. Lenk, H.-A. Krug von Nidda, C. Müller, M. Y. Kupriyanov, A. S. Sidorenko, S. Horn, R. Tidecks, and L. R. Tagirov, Phys. Rev. B **87**, 144507 (2013).

[19] G. Nowak, K. Westerholt, and H. Zabel, Supercond. Sci. Technol. **26**, 025004 (2013).

[20] X. L. Wang, A. Di Bernardo, N. Banerjee, A. Wells, F. S. Bergeret, M. G. Blamire, and J. W. A. Robinson, Phys. Rev. B **89**, 140508 (2014).

[21] A. A. Jara, C. Safranski, I. N. Krivorotov, C.-T. Wu, A. N. Malmi-Kakkada, O. T. Valls, and K. Halterman, Phys. Rev. B **89**, 184502 (2014).

[22] M. G. Flokstra, T. C. Cunningham, J. Kim, N. Satchell, G. Burnell, P. J. Curran, S. J. Bending, C. J. Kinane, J. F. K. Cooper, S. Langridge, A. Isidori, N. Pugach, M. Eschrig, and S. L. Lee, Phys. Rev. B **91**, 060501 (2015).

[23] Y. Gu, J. W. A. Robinson, M. Bianchetti, N. A. Stelmashenko, D. Astill, F. M. Grosche, J. L. MacManus-Driscoll, and M. G. Blamire, APL Mater. **2**, 046103 (2014).

[24] J. D. S. Witt, T. P. A. Hase, R. Fan, T. R. Charlton, S. Langridge, and M. G. Blamire, J. Phys. Condens. Matter **23**, 416006 (2011).

[25] L. Berbil-Bautista, S. Krause, M. Bode, and R. Wiesendanger, Phys. Rev. B **76**, 064411 (2007).

[26] J. W. A. Robinson, S. Piano, G. Burnell, C. Bell, and M. G. Blamire, Phys. Rev. B **76**, 094522 (2007).

[27] J. Stöhr and H. Siegmann, *Magnetism: From Fundamentals to Nanoscale Dynamics* (Springer-Verlag Berlin Heidelberg, 2006), Vol. 152. p. 534.

[28] F. J. Himpsel and B. Reihl, Phys. Rev. B **28**, 574 (1983).

[29] C. Santos, W. Nolting, and V. Eyert, Phys. Rev. B **69**, 214412 (2004).

[30] R. Wu, C. Li, A. J. Freeman, and C. L. Fu, Phys. Rev. B **44**, 9400 (1991).

[31] C. Schüßler-Langeheine, E. Weschke, C. Mazumdar, R. Meier, A. Y. Grigoriev, G. Kaindl, C. Sutter, D. Abernathy, G. Grübel, and M. Richter, Phys. Rev. Lett. **84**, 5624 (2000).

[32] D. Wegner, A. Bauer, A. Rehbein, and G. Kaindl, Jpn. J. Appl. Phys. **45**, 1941 (2006).

[33] J. Lang, Y. Baer, and P. Cox, J. Phys. F Met. Phys. **11**, 121 (1981).

[34] I. C. Moraru, W. P. Pratt, and N. O. Birge, Phys. Rev. B **74**, 220507 (2006).

[35] T. Y. Karminskaya and M. Y. Kupriyanov, JETP Lett. **85**, 286 (2007).

[36] T. Y. Karminskaya and M. Y. Kupriyanov, JETP Lett. **86**, 61 (2007).

[37] T. E. Golikova, F. Hübler, D. Beckmann, I. E. Batov, T. Y. Karminskaya, M. Y. Kupriyanov, A. A. Golubov, and V. V. Ryazanov, Phys. Rev. B **86**, 064416 (2012).

[38] A. J. Freeman in *Energy Band Structure, Indirect Exchange Interactions and Magnetic Ordering*, edited by R. J. Elloitt, *Magnetic Properties of Rare Earth Metals* (Plenum Publishing Corporation, 1972), p. 297.

[39] J. W. A. Robinson, J. D. S. Witt, and M. G. Blamire, Science (80-.). **329**, 59 (2010).

[40] N. Banerjee, C. B. Smiet, R. G. J. Smits, A. Ozaeta, F. S. Bergeret, M. G. Blamire, and J. W. A. Robinson, Nat. Commun. **5**, 3048 (2014).

[41] I. T. M. Usman, K. A. Yates, J. D. Moore, K. Morrison, V. K. Pecharsky, K. A. Gschneidner, T. Verhagen, J. Aarts, V. I. Zverev, J. W. A. Robinson, J. D. S. Witt, M. G. Blamire, and L. F. Cohen, Phys. Rev. B **83**, 144518 (2011).

[42] B. Li, N. Roschewsky, B. A. Assaf, M. Eich, M. Epstein-Martin, D. Heiman, M. Münzenberg, and J. S. Moodera, Phys. Rev. Lett. **110**, 097001 (2013).

[43] See supplemental material at [ ] for details of the modeling.

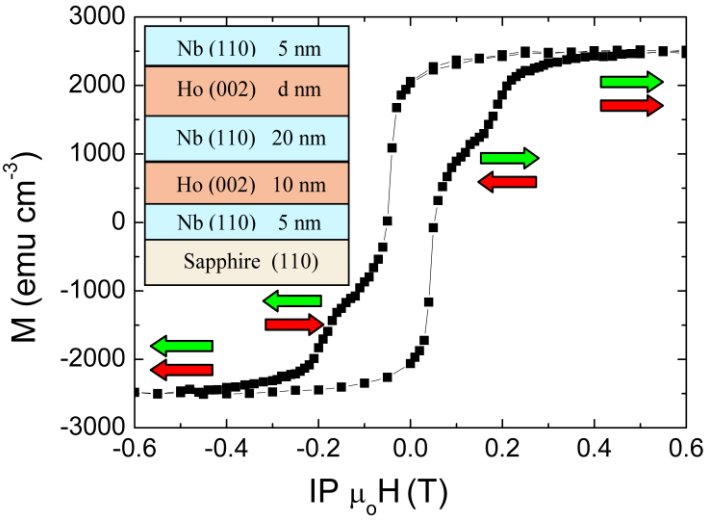

FIG. 1. (Color online) In-plane (IP) *M(H)* loop of a Ho (10 nm)/Nb (20 nm)/Ho (40 nm) SSV at 10 K. Arrows indicate the magnetization orientation of two epitaxial Ho films. Inset: The structure of an epitaxial multilayer with crystal orientations and thicknesses.

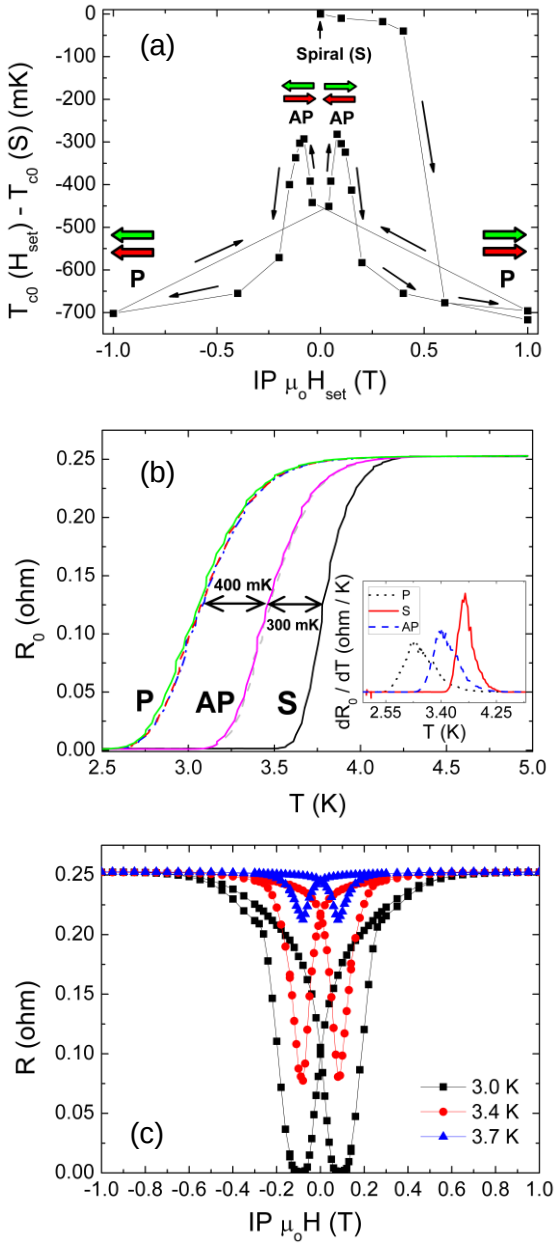

FIG. 2. (Color online) (a) Difference between the zero-field critical temperature following a set field and the as-cooled critical temperature for which the Ho is in the spin spiral state vs. set field ((T_{c0} (H_{set}) - T_{c0} (S) vs. $\mu_o H_{set}$) of a Ho (10 nm)/Nb (20 nm)/Ho (40 nm) SSV. (b) $R_0(T)$ curves of the SSV at different $\mu_o H_{set}$ (0T, ± 1 T and ± 0.1T) which correspond to different states (S, P, and AP). Inset: $dR_0(T)/dT$. (c) $R(H)$ measurements of the SSV at three different temperatures.

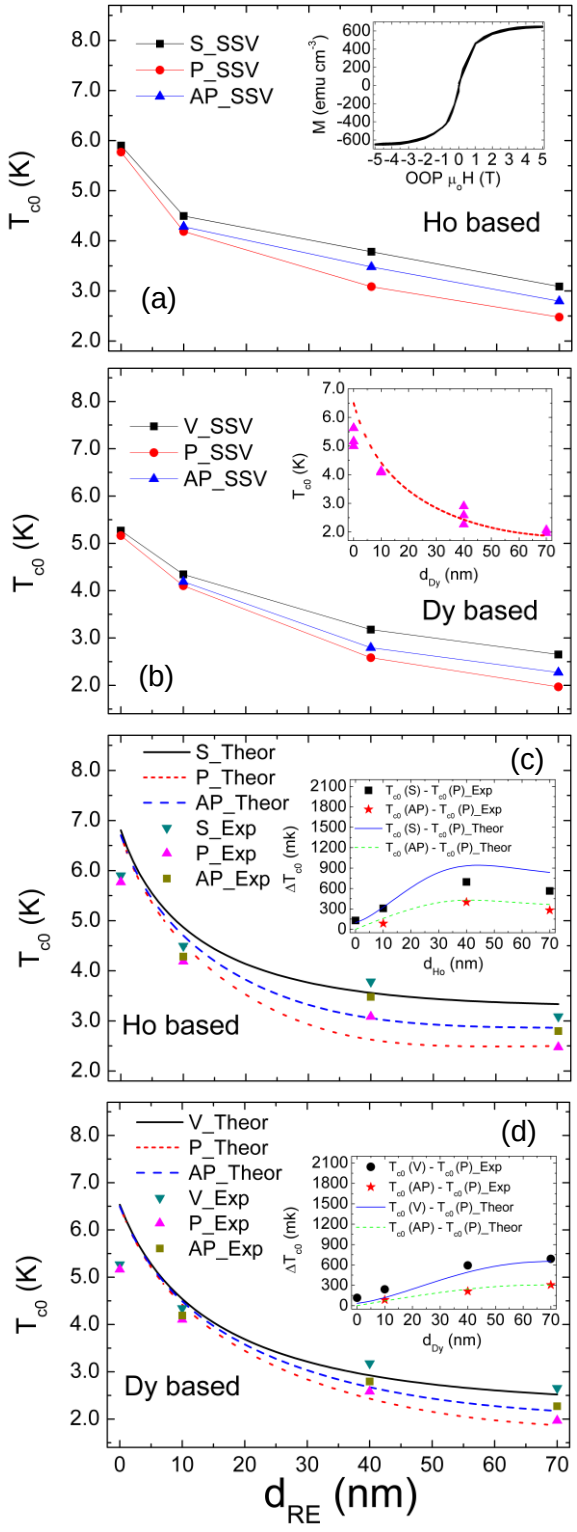

FIG. 3. (Color online) (a) Summary of T_{c0} for Ho-based SSVs (S: Spiral, P: Parallel, AP: Antiparallel). (b) Summary of T_{c0} for Dy-based SSVs (V: Virgin). (c) Comparison of experimental and theoretical results for Ho-based SSVs. (d) Comparison of experimental and theoretical results for Dy-based SSVs. Insets: (a) Out-of-plane (OOP) *M(H)* loop of a Ho (10 nm)/Nb (20 nm)/Ho (70 nm) SSV. (b) T_{c0} vs. d_{Dy} at P state. (c) ΔT_c in different states for Ho-based SSVs. (d) ΔT_c in different states for Dy-based SSVs.